to appear in Proc. IEEE/CIC ICCC

Reconfigurable Intelligent Surface-Aided Time Reversal Wireless Systems

Shimaa Naser*, Omar Alhussein*†, Lina Bariah‡, De Mi§, and Sami Muhaidat *†

*Khalifa University 6G Research Centre, Abu Dhabi, UAE
†Department of Systems and Computer Engineering, Carleton University, Ottawa, Canada
‡Technology Innovation Institute, 9639 Masdar City, Abu Dhabi, UAE
§Future Information Networks Research Cluster, College of Computing, Birmingham City University, UK
shimaa.naser@ku.ac.ae, omar.alhussein@ku.ac.ae, lina.bariah@ieee.org, de.mi@bcu.ac.uk, muhaidat@ieee.org

***Abstract*—Time reversal (TR) has the potential to revolutionize wireless communication, owning to its capabilities to focus the signal energy in both time and space domains. Nevertheless, its performance is highly affected by the richness of the multipath channel, which is highly degraded in sparse multipath environments. Therefore, in this paper, we aim to address this issue by leveraging reconfigurable intelligent surfaces (RISs) to artificially create rich scattering environments. We investigate the performance gain of RIS-assisted TR by adjusting the RIS parameters to efficiently realize artificially rich multipath fading. The simulation results demonstrate the effectiveness of integrating RIS with TR in sparse multipath environments, in terms of the bit error rate and channel capacity. Finally, we quantify the performance degradation of the proposed RIS-assisted TR under the effect of channel estimation errors. It is shown that imperfect channel state information has a significant impact on the performance of the proposed scheme.**

I. Introduction

The sixth generation (6G) of wireless communication is envisaged to support a plethora of data-hungry and delay-sensitive applications, which imposes further limitations on the network's performance in terms of reliability, latency, rate, and energy consumption. This has motivated the research community to explore higher frequency ranges, exceeding the millimeter-wave band, to satisfy the envisioned data rate requirements in 6G networks. Nevertheless, communication at higher frequencies requires energy-efficient radio frequency (RF) front ends design and computationally efficient signal processing techniques, which are still the main challenges to achieving the vision of 6G networks. In this context, time reversal (TR), a linear precoding technique, has been recently proposed for ultra-wideband (UWB) communications to pre-process the signals before transmission using the time-reversed (and conjugate if complex) channel impulse response (CIR). Such a filter has the capability to focus the energy of the signals, in a rich scattering environment, in both space and time domains at the intended receiver. It is worth noting that the time-focusing property of TR can assist in reducing the inter-symbol interference (ISI) that severely degrades the system performance in multipath environments. On the other hand, the spatial focusing property offers great potential for reducing multi-user interference and the intercept probability in the presence of eavesdroppers [1]. Therefore, the intended user receives high energy from all harvested multipath components without the need for complicated multi-antenna RF front ends at the receiver that requires heavy signal processing techniques. Thus, it is anticipated that TR will play a crucial role in supporting low-complexity, energy-efficient, and secure communications in future 6G networks.

The power density of the wireless signal received by the antenna is affected by multiple factors including multipath channels, shadowing effects, and large-scale path loss. As a consequence, only a fraction of the transmitted energy from the source can be successfully harvested at the energy harvesting receiver. Although multi-antenna techniques have been developed to tackle the limited power issue, incorporating additional RF chains can raise the overall implementation cost. Moreover, in indoor scenarios with rich scattering, multi-antenna processing schemes may not function properly due to the blockage caused by the obstacles. Therefore, TR is also deemed to boost the energy harvesting capabilities of wirelessly powered devices by making full use of the multipath propagation to sustain the received power at the harvester input.

Motivated by the promising capabilities of TR, several research works have investigated its performance in different contexts. The authors in [2], [3] studied the performance of TR communication in a UWB communication system under the assumption of perfect channel state information (CSI) at the transmitter. However, in practical scenarios, wireless channels may experience uncertainties, mainly due to the uplink and downlink noises, which highly affect the focusing gain and performance of TR. In the context of broadband systems, TR was also considered in [4]. However, compared to UWB systems, broadband systems encounter less scattering in the propagation channels. Thus, in cases where users are located in close proximity to each other, channels of different users experience high correlation. In such scenarios, the focusing gain of TR is highly degraded, which consequently degrades the system performance. Therefore, the authors in [5] quantified the channel capacity and the bit error rate (BER) performance of TR communication in multi-user UWB systems, while considering both spatial correlation and channel estimation errors (CEEs). It was demonstrated that both the spatial correlation

and CEEs significantly reduce the bandwidth efficiency of TR, Therefore, it must be fully considered in the system design. By focusing the signal toward a legitimate receiver, TR is also expected to enhance the secrecy of the communication. Thus, different attempts have investigated the performance of TR in the context of physical layer security [6], [7]. Finally, the authors in [8] experimentally demonstrated the spatiotemporal-focusing capability of TR at different carrier frequencies in the sub-6-GHz, mmWaves, and sub-THz.

Despite the promising potentials of TR, its performance highly depends on the number of multipath of the signal propagation environment. That is, the larger the number of multipaths, the better the focusing capability, and hence the better the system performance. Consequently, in sparse multipath channels, the performance of TR is significantly degraded. Recently, the reflective intelligent surface (RIS) paradigm has been widely investigated in the open literature due to its capabilities to control the propagation environment to extend the coverage and enhance the signal's quality, with minimal energy consumption [9]. RIS comprises a large number of small, low-cost, and passive elements, that reflect the incident signal with an adjustable phase shift and amplitude, enabling a wide range of functionalities, including beam focusing, splitting, reflection, and absorption.

Owning to the simple and low-cost implementation and low-power consumption features, as well as its capabilities to emulate rich multipaths by reflecting and exerting adjustable amplitude/phase changes on incident signals, RIS technology is regarded as an attractive candidate for supporting TR. With this motivation, in the present work, we investigate the integration of the newly emerged RIS technology with TR, aiming at improving the diversity of the signal propagation paths. Such work, to the best of the author's knowledge, has not been considered before in the open literature. Firstly, we provide a description of the system and signal models of RIS-assisted TR communication then, we define and evaluate a number of system performance metrics, including the channel capacity and BER. Furthermore, we examine the performance of the proposed framework and compare it with the baseline scheme where RIS is not employed. Subsequently, we investigate the impact of different parameters, such as the number of reflecting elements and the number of multipath components, on the performance of the proposed scheme. Finally, we consider a more practical scenario where the CSI is imperfectly estimated at the transmitter then, we quantify the performance degradation of the proposed RIS-assisted TR under such CEEs.

II. System and Signal Models

We consider a downlink system, which consists of a single-antenna user equipment (UE) and a base station (BS), as depicted in Fig. 1. Assuming that the direct link is blocked between the BS and UE, the BS communicates with the user with the aid of an RIS, that comprises R reflecting elements. The communication between the BS and the UE adopts the TR scheme. The distances between BS-RIS, RIS-UE, and BS-UE

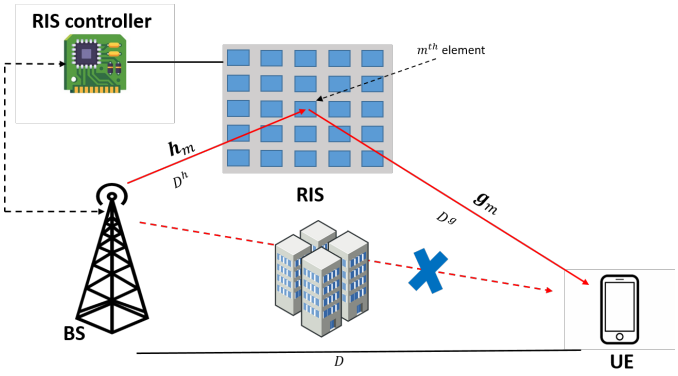

Fig. 1. System model for RIS-assisted communication.

are denoted by D^h, D^g, and D, respectively. Furthermore, we consider the case where the channels from the BS to the RIS and from the RIS to the UE are independent and identically distributed (IID) Rayleigh fading multipath channels. More specifically, $\mathbf{h}_r \in \mathbb{C}^{L_h \times 1}$ denotes the L_h-tap CIR of the link between the BS and the r^{th} reflecting element of the RIS. Similarly, $\mathbf{g}_r \in \mathbb{C}^{L_g \times 1}$ denotes the L_g-tap CIR of the link between the r^{th} reflecting element of the RIS and the UE. Each component of $\mathbf{h}_r$ and $\mathbf{g}_r$, i.e., $h_{r,l}$ and $g_{r,l}$, is the fading coefficient of the l^{th} path of the corresponding channel. In this work, we assume that the channel coefficients are circular symmetric complex Gaussian random variable (RV) with zero mean and the following variances

$$\sigma^2_{h_{r,l}} = E[|h_{r,l}|^2] = \eta_h \exp\{-lT_s/\tau_h\},\ l \in \{0, 1, ..., L_h - 1\}, \tag{1a}$$

$$\sigma^2_{g_{r,l}} = E[|g_{r,l}|^2] = \eta_g \exp\{-lT_s/\tau_g\},\ l \in \{0, 1, ..., L_g - 1\}, \tag{1b}$$

where T_s is the sampling period, τ_h and τ_g are the delay spread of the channels $\mathbf{h}_r$ and $\mathbf{g}_r$, respectively. Moreover, η_h and η_g denote the large-scale fading coefficients of the channels $\mathbf{h}_r$ and $\mathbf{g}_r$, respectively. It should be noted that for the case where the RIS is close to the BS or UE, the corresponding channel may be considered frequency-flat due to the small separation distances. To characterize the performance gain brought by the RIS and assuming channel reciprocity, the CSI of all involved channels are assumed to be perfectly known at the BS (cascaded channel estimation in RIS has been considered in the open literature through different approaches, such as compressive sensing, deep learning, and matrix factorization [10]). Therefore, the cascaded CIR corresponding to the r^{th} reflecting element $\mathbf{f}_r \in \mathbb{C}^{L_h + L_g - 1}$ is represented by the following

$$\mathbf{f}_r = \mathbf{h}_r \circledast \mathbf{g}_r, \tag{2}$$

where $\circledast$ denotes the convolution operation. At the first stage, the cascaded channels are estimated then, in the transmission stage, the user's signal is precoded using the time-reversed and conjugate version of the normalized cascaded CIR, before being sent. Consequently, the equivalent cascaded CIR

corresponds to the r^{th} reflecting element can be expressed as follows

$$\mathbf{f}_r^{eq} \triangleq [f_{r,0}^{eq}, f_{r,1}^{eq}, ..., f_{r,2(L_h+L_g-1)-2}^{eq}], \tag{3}$$

where $f_{r,n}^{eq}$ is the n^{th} multipath component of $\mathbf{f}_r^{eq}$, which is given by the following

$$f_{r,n}^{eq} = \frac{\sum_{l=0}^{L_h+L_g-2} f_{r,l} \cdot f_{r,L_h+L_g-2-n+l}^{*}}{\sqrt{\sum_{l=0}^{L_h+L_g-2} |f_{r,l}|^2}},$$
$$n = 0, 1, ..., 2(L_h + L_g - 1) - 2. \tag{4}$$

At the RIS, each element re-scatters the received signal with different reflection coefficients $\phi = [\phi_1, \phi_2, ..., \phi_R]^T$, where $\phi_r = \beta_r e^{j\theta_r}$ with $\beta_r \in [0, 1]$ and $\theta_r \in [0, 2\pi]$ denote the amplitude coefficient and the phase shift of the r^{th} element, respectively. Following the literature for lossless metasurfaces, we set $\beta_r = 1$ in the sequel of this paper. Hence, the received signal at UE through the RIS is written as follows

$$\mathbf{y} = \sqrt{P_x} \sum_{r=1}^{R} \mathbf{f}_r^{eq} \circledast \mathbf{x}\, e^{j\theta_r} + \mathbf{z} \tag{5}$$

where P_x, $\mathbf{x}$, and $\mathbf{z}$ represent the transmit power, vector of the transmitted symbols, and the additive white Gaussian noise (AWGN) with zero mean and σ^2 variance, respectively. By expanding (5), the n^{th} received sample y_n can be written as follows

$$y_n = \sqrt{P_x} \sum_{r=1}^{R} f_{r,L_h+L_g-2}^{eq}\, x_{n-(L_h+L_g-2)}\, e^{j\theta_r} + \sqrt{P_x} \sum_{r=1}^{R} \sum_{\substack{i=0,\\ i\neq L_h+L_g-2}}^{2(L_h+L_g-1)-2} f_{r,i}^{eq}\, x_{n-i}\, e^{j\theta_r} + z_n. \tag{6}$$

It can be noted from (4) that at sample $n = L_h + L_g - 2$, the term $f_{r,L_h+L_g-2}^{eq}$ is equivalent to $\sqrt{\sum_{l=0}^{L_h+L_g-2} |f_{r,l}|^2}$. Thus, (6) can be further rewritten as follows

$$y_n = \sqrt{P_x} \sum_{r=1}^{R} \sqrt{\sum_{l=0}^{L_h+L_g-2} |f_{r,l}|^2}\, x_{n-(L_h+L_g-2)}\, e^{j\theta_r} + \sqrt{P_x} \sum_{r=1}^{R} \sum_{\substack{i=0,\\ i\neq L_h+L_g-2}}^{2(L_h+L_g-1)-2} f_{r,i}^{eq}\, x_{n-i}\, e^{j\theta_r} + z_n. \tag{7}$$

It is noted from (7) that the first term on the right-hand side represents the useful signal where the energy is being focused at sample $n = L_h+L_g-2$ of the equivalent cascaded CIR, i.e., $f_{r,L_h+L_g-2}^{eq}$, this is because different copies of the transmitted signal add up coherently as all components have zero phases. On the other hand, the second term represents the induced ISI, where different components are added incoherently, thus, the ISI effect can be mitigated. Furthermore, it is noted that the energy of the desired signal at sample $n = L_h + L_g - 2$ is maximized by setting the angles of the reflecting element to zero.

TABLE I: Simulation parameters.

Parameter	Symbol	Value
BS-UE distance	D	$55\ m$
BS-UE channel taps	L	2
BS-RIS distance	D^h	$5\ m$
RIS-UE distance	D^g	$50\ m$
Reference distance	D_0	$1\ m$
Path loss exponent BS-RIS link	α_h	2
Path loss exponent RIS-UE link	α_g	2.7
Ratio of non-negligible path power to the first path power	A	-20 dB
Bandwidth	B	10 MHz
Noise variance	σ^2	90 dBm

To quantify the performance gain of the proposed RIS-assisted TR system, channel capacity is an important metric to be considered. It presents the information rate achieved per unit bandwidth as the following

$$C = \log_2(1 + \gamma), \tag{8}$$

where γ is the signal-to-interference-plus-noise ratio (SINR) which can be written, using (7), as follows

$$\gamma = \frac{P_x \left| \sum_{r=1}^{R} \sqrt{\sum_{l=0}^{L_h+L_g-2} |f_{r,l}|^2} \right|^2}{P_x \sum_{\substack{i=0,\\ i\neq L_h+L_g-2}}^{2(L_h+L_g-1)-2} \left| \sum_{r=1}^{R} f_{r,i}^{eq} \right|^2 + \sigma^2}. \tag{9}$$

As mentioned earlier, the performance of RIS-assisted TR system is highly affected by the accuracy of the estimated cascaded BS-RIS-UE CIR at the transmitter. Nevertheless, in practical scenarios, CSI estimation encounters uncertainties that degrade system performance. In this work, statistical CSI the error model is adopted to take into account the effect of CEE, where the estimated cascaded CIR corresponds to the r^{th} element is represented by the following

$$\hat{\mathbf{f}}_r = \mathbf{f}_r + \mathbf{e}_r, \tag{10}$$

where $\hat{\mathbf{f}}_r$ represents the estimated channel and $\mathbf{e}_r$ is the estimation error, which is assumed to be uncorrelated. Thus, the variances of the different involved random variables in (10) are given as follows [5]

$$E[|\hat{f}_{r,l}|^2] = E[|f_{r,l}|^2] + E[|e_{r,l}|^2]. \tag{11a}$$
$$E[|e_{r,l}|^2] = \epsilon E[|f_{r,l}|^2], \tag{11b}$$

where ϵ denotes the error factor.

III. Simulation Results

This section shows numerical results in order to demonstrate the achievable performance of the considered RIS-assisted TR communication system. To this end, we assume that the BS and UE are separated by distance $D = 55\ m$ and the RIS comprises either $R = 4$, 8, 16, 32 elements. The large-scale fading coefficients η_h and η_g are calculated according to the

following; $\eta_h = \eta_0(D^h/D_0)^{-\alpha_h}$ and $\eta_g = \eta_0(D^g/D_0)^{-\alpha_g}$, where D_0 is the reference distance set to 1 m, $D^h = 5$ m, $D^g = 50$ m, and η_0 is the path loss at the reference distance chosen as -30 dB for each individual link [11]. Also, α_h and α_g denote the path loss exponents for the links between the BS-RIS and the RIS-UE, which are set as 2 and 2.7, respectively. Furthermore, the bandwidth B is set to 10 MHz, while the number of taps L_h and L_g, without loss of generality and unless otherwise stated, are chosen as $L_h = L_g = 2$, where the tap of each channel is a complex Gaussian RV with zero mean and variances calculated according to (1a) and(1b). The RMS delay spread of each link is calculated as $\tau_h = -T_s.(L_h - 1)/\log A$ and $\tau_g = -T_s.(L_g - 1)/\log A$, where $T_s = 1/B$, and A is the ratio of non-negligible path power to the first path power which is set to -20 dB [12]. In the simulation, a total of 10^5 channel realizations are randomly generated to evaluate the average performance of the considered RIS-assisted TR communication system in terms of the BER and channel capacity. Finally, the noise variance σ^2 is set to -90 dBm. For convenience, a summary of the used parameters is depicted in Table I.

Fig. 2 studies the BER performance of RIS-assisted TR system for binary phase shift keying (BPSK) modulation and for a different number of reflecting elements R. Additionally, to emphasize the performance gain obtained by integrating RIS technology with TR communication, we compare the performance with the baseline scheme where RIS is not employed. It is noted from the figure that, using RIS provides an enhancement on the BER performance of TR system without RIS in a sparse multipath environment. For instance, at $P_x = 20$ dBm and $R = 16$, almost 98.48% improvement on the BER is achieved. Thanks to the RIS ability to artificially create additional multipath components in the propagation environment between the BS and UE. However, it is noted that for $R = 4$, the RIS size is not sufficient to remove the ISI and improve the desired signal term, which explains the performance gap compared to the case where RIS is not employed. Nevertheless, increasing the number of the RIS elements further improves the diversity gain, and hence, the BER performance. It can be noted that the performance of the TR system without RIS tends to saturate at high transmit powers due to the increased power of the ISI component. To further emphasize on the usefulness of the proposed scheme, we compare its performance with the scenario where the RIS is employed without utilizing TR at the BS. In this regard, the RIS elements compensate for the phase of the strongest channel tap as proposed in [13]. Fig. 3 shows that integrating TR with RIS technology achieves a significant performance enhancement compared to the case where TR is not employed at the BS. Moreover, it is noted that the performance of the RIS system without TR degrades as the number of channel taps increases, due to the increased ISI. On the other hand, in the case where RIS is integrated with TR, the performance gets improved with the number of channel taps due to the increased focusing gain.

Next, in Fig. 4, we investigate the effect of the number

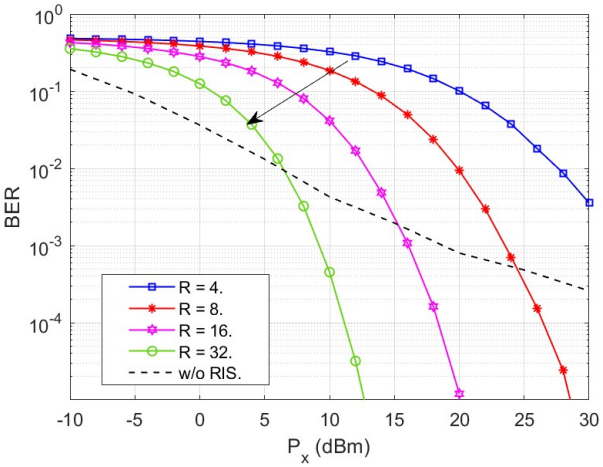

Fig. 2. BER performance of RIS-assisted TR communication system versus transmit power and for the different number of reflecting elements R. $L_h = L_g = 2$.

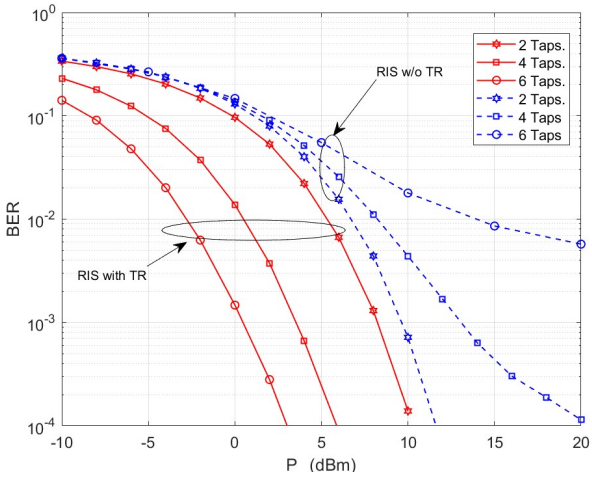

Fig. 3. BER performance comparison of RIS with and without utilizing TR communication. $R = 32$. $A = -10$ dB.

of channel taps on the BER performance of the proposed RIS-assisted TR system. For the different considered numbers of RIS elements, BER is highly affected by the number of taps. That is, the larger the number of taps, the lower the achieved BER, which is attributed to the improved diversity gain and focusing property that enhances the quality of the received signal. Furthermore, it is observed that increasing the number of the RIS elements can significantly improve the BER performance with less number of taps compared to small number of RIS elements. For instance, the achieved BER for a channel with 6 taps by using $R = 32,\ 16,\ 8$, and 4, are 1.8×10^{-4}, 0.0241, 0.151, 0.3, respectively. Thus, integrating RIS comprises large number of reflecting elements with TR would compensate for the performance degradation in sparse multipath environments, by artificially generating additional multipaths in the signal's propagation environments. Nevertheless, it is noted from the figure that the BER performance saturates as the number of channel taps increases since both the

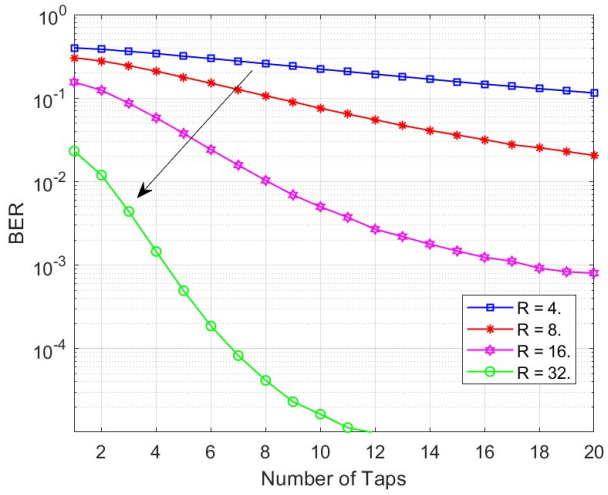

Fig. 4. BER performance of RIS-assisted TR communication system versus number of channel taps and for different number of reflecting elements R. $P_x = 5$ dBm.

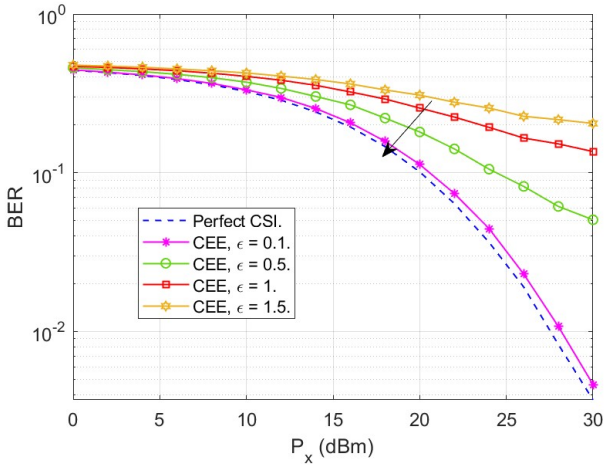

Fig. 6. Effect of channel estimation error on the performance of RIS-assisted TR communication system. $L_h = L_g = 2.$, $R = 4$.

desired signal power and the ISI power increase proportionally with the number of taps.

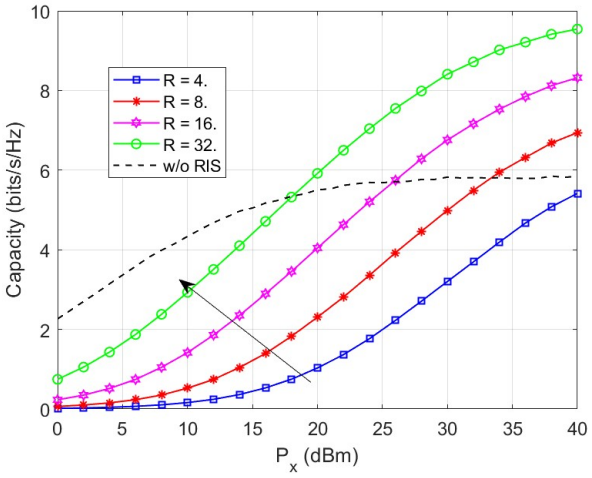

Fig. 5. Capacity of RIS-assisted TR communication versus transmit power and for different numbers of reflecting elements. $L_h = L_g = 2$.

Subsequently, in Fig. 5 we study the channel capacity performance of the proposed RIS-assisted TR system for different numbers of RIS elements. It is obvious from the figure that the performance of TR with RIS outperforms the scenario without RIS especially for a large number of RIS elements and high transmit power. Since the desired signal power and the ISI power increase proportionally with the transmit power, the capacity saturates at high transmit power values. Finally, we investigate the effect of the CEE on the performance of the proposed scheme in Fig. 6. It is noted that the performance is highly degraded as the estimation error factor ϵ increases, where it saturates at high transmit power P_x due to the loss of signal focusing property. For instance, the BER performance loss is almost 92.67% at $\epsilon = 0.5$ and transmit power 30 dBm. Hence, it becomes evident that channel estimation errors should not be neglected in practical implementation scenarios of RIS-assisted TR systems, yet they should be taken into consideration through different RIS element phases design.

Despite the advantages of integrating RIS with TR systems, real-world scenarios involve several practical challenges and limitations that need to be carefully addressed to realize the full potential of RIS-assisted TR. For example, the careful deployment of RIS units is crucial to ensure optimal coverage and reflection angles, which might necessitate structural modifications to existing infrastructure. Although RIS units typically consume low power, maintaining a consistent and reliable power supply, especially in outdoor or remote locations, is essential. In such cases, integrating energy harvesting techniques with RIS-assisted systems can provide continuous energy replenishment by scavenging and converting ambient energy sources into electrical energy to power the RIS circuit. Another practical concern is ensuring connectivity for control signals to adjust RIS parameters. Practical RIS elements have limited phase resolution due to quantization, leading to suboptimal phase adjustments. This deviation from perfect phase control can reduce the effectiveness of RIS in focusing and steering signals.

Moreover, the performance of RIS-assisted systems heavily depends on the accuracy of the Channel State Information (CSI), which is challenging due to channel estimation errors, feedback delays, and the dynamic nature of wireless channels. The process of CSI estimation and subsequent optimization of RIS phases can be computationally intensive, requiring efficient algorithms and significant processing power for real-time operation, which can be a limitation in resource-constrained environments.

In summary, future work should focus on robust CSI estimation techniques, efficient RIS deployment strategies, and realistic performance evaluations under non-ideal conditions to help understand and harness the potential of RIS-assisted TR systems in practical scenarios

IV. Conclusion

In this paper, we investigated the performance of RIS-assisted time reversal (TR) communication systems in sparse multipath frequency selective channels. Specifically, we tackled the focus gain degradation issue of TR in such environments by leveraging RIS to artificially create rich multipath in the signal's propagation environments. Furthermore, we considered the practical scenario where the channel state information estimation encounters uncertainties that degrades system performance. Simulation results demonstrated the ability of RIS to enhance the performance of TR in terms of the achieved BER and capacity. Additionally, it has been shown that the achieved BER degrades with the channel estimation error because of the loss of signal focusing gain. Thus, channel estimation errors in RIS-assisted TR systems have to be fully considered by developing compensation mechanisms for the phase noise to enhance the focusing gain in practical implementation.

References

[1] F. Han, Y.-H. Yang, B. Wang, Y. Wu, and K. J. R. Liu, "Time-reversal division multiple access over multi-path channels," *IEEE Transactions on Communications*, vol. 60, no. 7, pp. 1953–1965, May 2012.

[2] H. Ma, B. Wang, Y. Chen, and K. J. R. Liu, "Waveforming optimizations for time-reversal cloud radio access networks," *IEEE Transactions on Communications*, vol. 66, no. 1, pp. 382–393, Jan. 2018.

[3] A. Dezfooliyan and A. M. Weiner, "Spatiotemporal focusing of phase compensation and time reversal in ultrawideband systems with limited rate feedback," *IEEE Transactions on Vehicular Technology*, vol. 65, no. 4, pp. 1998–2006, April 2016.

[4] M.-A. Bouzigues, I. Siaud, M. Helard, and A.-M. Ulmer-Moll, "Turn back the clock: Time reversal for green radio communications," *IEEE Vehicular Technology Magazine*, vol. 8, no. 1, pp. 49–56, March 2013.

[5] B. He, T. Sun, Z. Wang, and K. Su, "A fine-grained analysis of time reversal MU-MISO systems over correlated multipath channels with imperfect CSI," *IEEE Access*, vol. 6, pp. 69 516–69 527, 2018.

[6] R. Zhao, M. Khalid, O. A. Dobre, and X. Wang, "Physical layer node authentication in underwater acoustic sensor networks using time-reversal," *IEEE Sensors Journal*, vol. 22, no. 4, pp. 3796–3809, 2022.

[7] S. J. Golstein, F. Rottenberg, F. Horlin, P. De Doncker, and J. Sarrazin, "Physical layer security in an OFDM time reversal SISO communication with imperfect channel state information," *IEEE Access*, vol. 10, pp. 26 778–26 794, 2022.

[8] G. C. Alexandropoulos, A. Mokh, R. Khayatzadeh, J. de Rosny, M. Kamoun, A. Ourir, A. Tourin, M. Fink, and M. Debbah, "Time reversal for 6G spatiotemporal focusing: Recent experiments, opportunities, and challenges," *IEEE Vehicular Technology Magazine*, vol. 17, no. 4, pp. 74–82, Dec. 2022.

[9] E. Basar, M. Di Renzo, J. De Rosny, M. Debbah, M.-S. Alouini, and R. Zhang, "Wireless communications through reconfigurable intelligent surfaces," *IEEE Access*, vol. 7, pp. 116 753–116 773, 2019.

[10] C. Pan, G. Zhou, K. Zhi, S. Hong, T. Wu, Y. Pan, H. Ren, M. D. Renzo, A. Lee Swindlehurst, R. Zhang, and A. Y. Zhang, "An overview of signal processing techniques for RIS/IRS-aided wireless systems," *IEEE Journal of Selected Topics in Signal Processing*, vol. 16, no. 5, pp. 883–917, Aug. 2022.

[11] Q. Li, M. Wen, E. Basar, G. C. Alexandropoulos, K. J. Kim, and H. Vincent Poor, "Channel estimation and multipath diversity reception for ris-empowered broadband wireless systems based on cyclic-prefixed single-carrier transmission," *IEEE Transactions on Wireless Communications*, pp. 1–1, 2023.

[12] Y. Cho, J. Kim, W. Yang, and C. Kang, *MIMO-OFDM Wireless Communications with MATLAB*, ser. IEEE Press. Wiley, 2010. [Online]. Available: https://books.google.ae/books?id=6HwAoeuMr3kC

[13] E. Arslan, I. Yildirim, F. Kilinc, and E. Basar, "Over-the-air equalization with reconfigurable intelligent surfaces," *IET Communications*, vol. 16, no. 13, pp. 1486–1497, Jun. 2022. [Online]. Available: https://ietresearch.onlinelibrary.wiley.com/doi/abs/10.1049/cmu2.12425